

## Hemodynamic and Flow Recirculation Effect on Rupture Prediction of Middle Cerebral Artery Aneurysm

Open  
Access

Nadia Shaira Shafii<sup>1</sup>, Ryuhei Yamaguchi<sup>3</sup>, Ahmad Zahran Md Khudzari<sup>1,2</sup>, Gaku Tanaka<sup>4</sup>, Atsushi Saitoh<sup>5</sup>, Makoto Ohta<sup>3</sup>, Kahar Osman<sup>1,2,\*</sup>

<sup>1</sup> School of Biomedical Engineering and Health Sciences, Faculty of Engineering, Universiti Teknologi Malaysia, Johor Bahru, Malaysia

<sup>2</sup> IJN-UTM Cardiovascular Engineering Center, Universiti Teknologi Malaysia, Johor Bahru, Malaysia

<sup>3</sup> Institute of Fluid Science, Tohoku University, Miyagi, Japan

<sup>4</sup> Graduate School of Engineering, Chiba University, Chiba, Japan

<sup>5</sup> Department of Neurosurgery, Sendai Medical Center, Miyagi, Japan

### ARTICLE INFO

### ABSTRACT

#### Article history:

Received 7 July 2020

Received in revised form 15 November 2020

Accepted 20 November 2020

Available online 12 December 2020

The mortality and morbidity rate due to the severe effect of intracranial aneurysm (IA) is increasing, which has driven research trend on aneurysm rupture risk. By understanding the nature and causes of the aneurysm rupture, preventive measures could be taken in avoiding rupture besides recommending proper treatments such as endovascular coiling. However, the presence of flow recirculation causes the aneurysm wall to degenerate and weakened. The weakened wall is due to the haemodynamic factors such as velocity, wall shear stress (WSS), time average WSS (TAWSS), OSI and RRT, which were analysed in this study. In the present study, the flow model simulated a human patient-specific aneurysm at the apex of the bifurcation in the middle cerebral artery (MCA) in the transient state. Experimental results of full-scale models were collected on a median, side plane to study the flow behaviour and validation to the numerical simulation settings, which resulted in good agreement with only 8% difference. The simulation results obtained showed several interesting findings. The jet flow into the aneurysm led to complex vortex formation due to impinging flow behaviour within the aneurysm dome. Additionally, the area that recorded low velocity was at 30% of low TAWSS with only 1% of OSI that was more than 0.3, while the OSI critical value and 0.27% area exceeded RRT threshold, which caused the large oscillating blood flow direction and activated the atherosclerosis progression. These results suggest that the jet flow into the dome may cause further damage to the wall of the MCA aneurysm, which will help in providing an insight towards completing a guidance system assessment of rupture risk for medical practitioners in future work.

#### Keywords:

Cerebral Aneurysm; Pulsatile Flow; Flow Recirculation; Particle Image Velocimetry; Computational Fluid Dynamics

Copyright © 2021 PENERBIT AKADEMIA BARU - All rights reserved

\* Corresponding author.

E-mail address: [kaharosman@utm.my](mailto:kaharosman@utm.my)

<https://doi.org/10.37934/arfmts.79.1.116>

## 1. Introduction

Intracranial aneurysms (IAs) are balloon-like dilations of the intracranial arterial wall in the brain. In the United States, 3 to 5 million people have been identified with intracranial wall dilation in which the wall becomes weaker due to flow irregularity. However, the symptoms are usually neglected or left unnoticed [1]. Japan had also reported a huge number of IAs. The rupture of IA leads to subarachnoid haemorrhage (SAH), which causes fatality in 40-50% of the cases and significant disability in 30% of cases [1]. In Japan, the incidence and mortality rates for SAH are 23 and 9 per 100 000 populations for all ages, respectively, whereas the annual rupture rate is ~2.7% [2]. Commonly, 3% of untreated people with brain aneurysm are at risk of bleeding. Aneurysm can happen in multiple locations of Circle of Willis [3,4].

In this study, the saccular aneurysm in middle cerebral artery (MCA) was chosen since this type of aneurysm was reported to have higher wall shear stress (WSS) and prone to rupture in comparison with the fusiform aneurysm. Furthermore, 90% of the aneurysm is commonly in saccular type [5]. It has been reported with animal experiments that high WSS has a close relationship with the initiation of cerebral aneurysm while low WSS causes rupture due to wall degradation [6,7]. The WSS might also play an important role in the rupture of cerebral aneurysms. Figure 1 shows several examples of patient-specific MCA saccular aneurysm [8]. Various sizes of aneurysm were considered especially the neck size since it is one of the factors that also cause complications during coiling treatment and affect the thrombosis issue [9].

The formation of aneurysm is generally due to the dysfunction of endothelial cells. The hemodynamic stress will increase from unhealthy practices such as taking alcohol, smoking and other biological factors such as female gender, infection, lipid and cholesterol accumulation, which then cause the normal endothelial cells and internal elastic lamina to become inflamed. Then, this inflammation will lead to the dysfunction of remodelling extracellular matrix for smooth muscle cell and initiate the aneurysm formation. Further inflammation will degenerate extremely and slowly cause the aneurysm to rupture. This will then affect other parameters and conditions such as low wall shear stress, media thinning and intraluminal thrombus. Figure 2 explains the analogy of aneurysm growth and rupture once the vessel is inflamed [7].

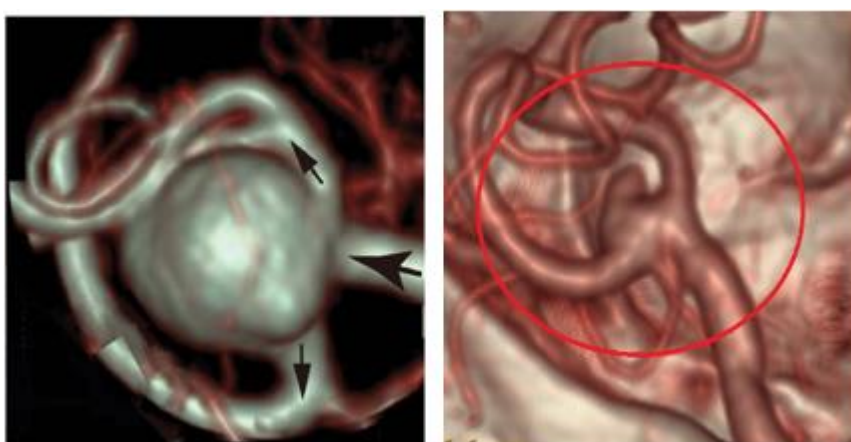


**Fig. 1.** Example of the patient-specific MCA saccular aneurysm images

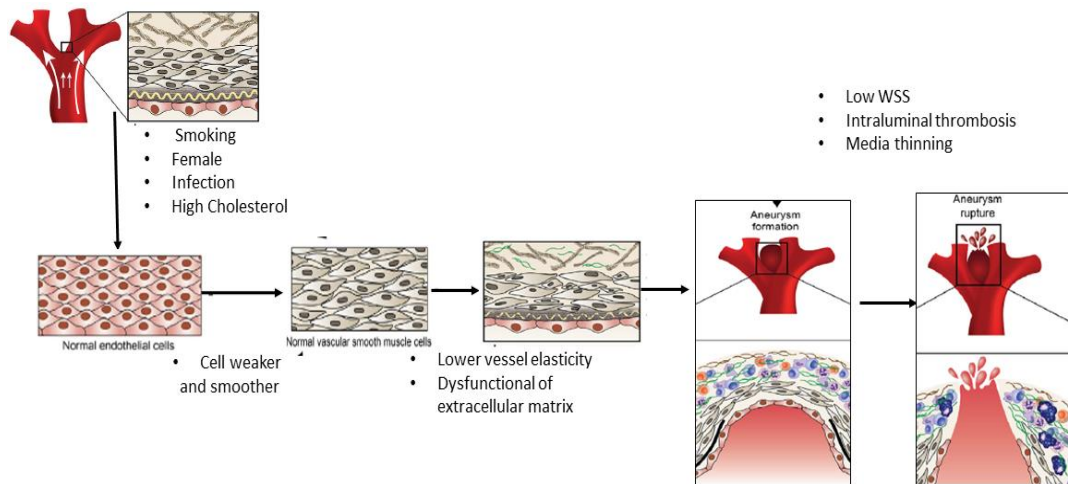


**Fig. 2.** Growth and rupture of aneurysm due to inflammation [7]

To avoid aneurysm from ruptures, surgical clipping or interventional neuroradiology can be done even though it still has morbidity and mortality risk [10]. The blood coagulation will be promoted and increased after undergoing the treatment, which helps to avoid the impinging blood flow to the vessel wall that will retard an aneurysm from rupturing [11]. The brain aneurysm rupture rate is increasing now up to one rupture in every 18 minutes due to the difficulties for the surgeons to make a decision due to the uncertainty on brain aneurysm rupture risk. Many people died before entering the operation or treatment room since they do not have accurate assessment to assist the physicians to balance the surgery risk and MCA aneurysm rupture [12]. Usually, the large size of an aneurysm has a high potential of rupture, but recent studies indicated that most of the ruptured aneurysms cases were in small size [13,14]. There were also qualitative factors that affect the rupture risk such as gender, age and location. Most of recent studies focused on the rupture in the brain aneurysm due to the morphologies impact and wall shear stress [15-17]. The impact of irregularity flow such as vortex formation and flow recirculation also contribute to the aneurysm wall thinning, which increases the risk of aneurysm to burst. Computational fluid dynamics (CFD) technique is the most prominent technique use to easily visualise and quantify the effects of flow behaviour. There were several researches that used CFD in their research focusing on flow behaviour such as Mustafa *et al.*, [18] who investigated the vortex shedding and proved secondary vortices related to the oscillating flow effects. In addition, Hamad *et al.*, [19] discussed about the fluid flow recirculation for water flow distribution application using CFD. Also, Cebra *et al.*, [20] claimed that slow swirling flow with low and oscillating wall shear stress led to atherosclerotic changes using their own in-house software. Thus, the objective of this present work is to show the presence of flow recirculation inside the patient-specific MCA aneurysm qualitatively with transient flow condition to mimic the blood flow inside their brain. These flow vortices happened due to the impinging effects of the jet flow into the aneurysm sac that weakened the wall, which then expedited the rupture process. This phenomenon was then supported quantitatively by several hemodynamic parameters considered namely wall shear stress, velocity, pressure, oscillatory shear index (OSI) and relative residence time (RRT), which triggered the rupture of the aneurysm [17,21,22]. Thus, in this study, it was hypothesised that these haemodynamic factors are due to the vortex's formation, which will be terminated by the recirculation of flow inside the bulge area that will increase the aneurysm rupture risk [22]. The flow recirculation will be on the result and discussion part.

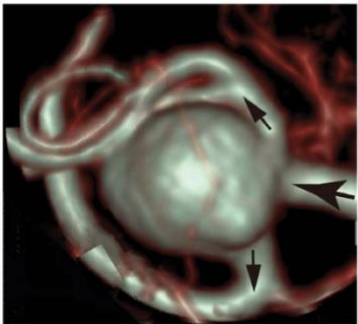
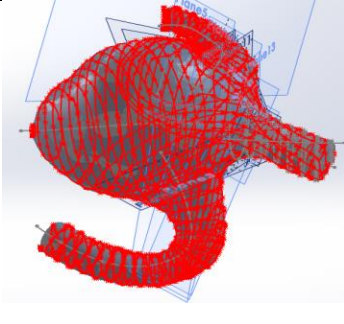
## 2. Methodology

### 2.1 Numerical Simulation

In this study, ANSYS CFD 19.1 software (Canonsburg, PA, USA) was used to simulate the patient-specific rigid model. The interaction with the surfaces defined by boundary condition was simulated using the computers. Therefore, fluid flow was simulated in an environment that provides reasonably reliable and accurate solutions across a wide range of applications. The solver was based on the finite volume method with several types of arbitrary mesh topologies such as hexahedral, tetrahedral, wedge and pyramid elements. The conservation of mass and momentum was the physical law used in this study.

The geometry of an MCA aneurysm was reconstructed using SOLIDWORKS (Dassault Systems SolidWorks Corporation, Waltham, MA) based on patient-specific model. The mesh generation and boundary condition setup of the model was exported to ANSYS CFD Fluent (Canonsburg, PA, USA) as in Table 1. There were three sub-steps in the reconstruction process before numerical simulation was carried out and the pulsatile inlet was used.

**Table 1**  
 The patient-specific model reconstruction process

Patient-specific model	Polyline creation from 3D images	Knit and combine the surface in Solid work
		

A transient velocity waveform for was imposed as inlet based on previous study as shown in Figure 5(a) [21]. Non-slip boundary condition was imposed on the walls and laminar flow model was selected since it has low Reynold number and this paper focused more on the flow characteristics away from the wall. Further in this case, there were not many differences between laminar and turbulent SST turbulent model as in previous work [24]. Also, the blood used in this simulation was considered as incompressible Newtonian fluid with density of 1188 kg/m<sup>3</sup> and 0.0035 N. s/m<sup>2</sup> for viscosity. Previous research recommended tuning to use the non-Newtonian blood behaviour to avoid overestimation as recommended, but this study was at an early stage to establish a guidance system for MCA aneurysm rupture risk. But the non-Newtonian blood behaviour will be considered for next stage of this research considering to increase the result accuracy [25]. Thus, the Newtonian blood behaviour to easy the experimental validation process in preparing the blood mimics fluid. The Navier-Stokes equation used in this simulation was expressed as Eq. (1).

$$\rho \frac{Du}{Dt} = -\nabla p + \mu \nabla^2 u + \rho g \quad (1)$$

where  $\rho$  is density,  $u$  is flow velocity,  $p$  is pressure,  $t$  is time,  $g$  is body acceleration,  $\mu$  is viscosity and  $\nabla$  is the divergence. Reynold number was based on the peak of velocity waveform as in Figure 3(a).

The maximum and minimum Reynolds numbers were 700 and 250, respectively, based on waveform used as in Figure 3(a). The flow rate was maintained at the same free flow rate in both outlet vessels. The mean Reynolds number of 310 was referred to as the flow rate of  $Q_{\text{mean}} = 300 \text{ mL/min}$ . The inlet waveform was simulated from [26]. One period of pulsatile flow was set to be 1.0 s, while the peak flow phase was at  $t = 0.25 \text{ s}$  and the Womersley number was  $\alpha = 1.86$ . Although the pulsatile flow waveform is simply simulated as in Table 1, the flow rate through both outlets was free flow. This transient flow simulation was run from two cycles to avoid any unstable pulsatile flow effect related to flow initialisation. The simulation data was validated to the experimental data quantitatively and qualitatively to discuss the flow complexity in 3D view.

The model geometry was divided into three boundary zones: the inflow, impeller region and the volume region. A triangular mesh (tetrahedral) was selected for the entire flow domain as the quality of mesh has a significant impact on the accuracy of the numerical solutions. The meshing setting used involved 663 608 nodes and 1817468 elements. This grid setting was chosen based on grid independent test (GIT) on different node numbers where there was no significant number of velocity changes at the optimum node number. Figures below shows the comparison between numbers of node and the velocity. Meanwhile, the graph generated in CFD Post below shows three numbers of nodes used, which were 350 k nodes, 450 k nodes and 560 k nodes. Based on the velocity result of each nodes number, there was no significant velocity value changed even as the node numbers increases past 100 k nodes as shown in Figure 3(b). Figure 4 shows the unstructured meshing of tetrahedral elements used. The meshing distribution density was a bit higher near the wall compared to the other regions. To ensure the adequate overall mesh quality, the skewness and aspect ratio were used as mesh quality indicators by more than 90%.

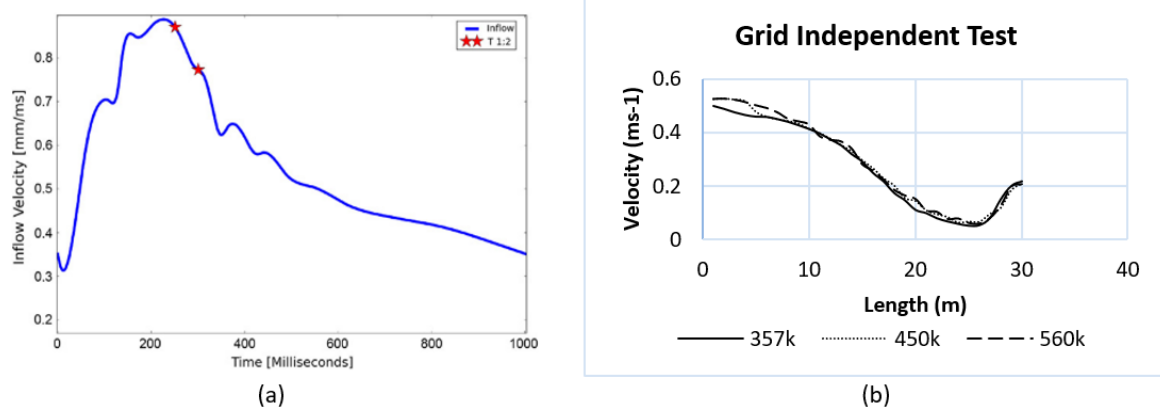


**Fig. 3.** (a) Inlet waveform [26]; (b) GIT validation

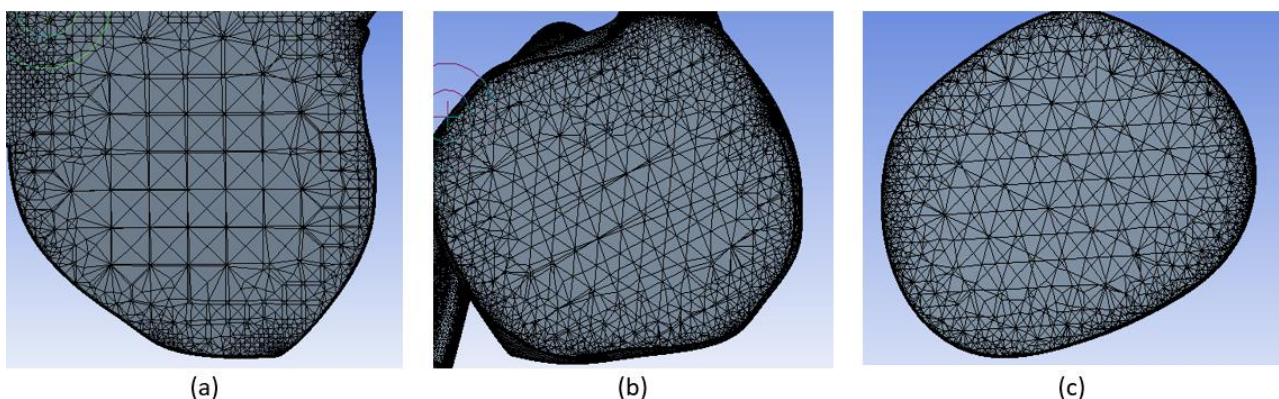


**Fig. 4.** Meshing of the MCA aneurysm on (a) median plane (b) side plane and (c) top plane

## 2.2 Particle Image Velocimetry Set Up

An experimental rig with transient flow and non-scale up silicone phantom model was set up to validate the simulation results using Particle Image Velocimetry (PIV) technique. The PIV setting was referred to a previous work [27]. The velocity vector was measured by two-dimensional PIV using a 15 Hz Double Pulse Yag Laser Solo II (New Wave Research Ltd., CA, USA) with a pulse interval of 20  $\mu$ s, an image intense charged-coupled device camera ( $1376 \times 1040$  pixels; Lavisision, Göttingen, Germany), a 2 W continuous Yag Laser (Dantec SYSTEM 8, Copenhagen, Denmark) and a SpeedSense M camera (Dantec SYSTEM 8). The measurement was performed at the median xy plane under 1000 fps. The interrogation window size was 12 pixels circular with an overlap of 50%.

### 2.2.1 Silicone phantom preparation

To prepare the phantom aneurysm model, the aneurysm mould was firstly fabricated as shown in Figure 5. Secondly, the mould was dipped into the silicone and rotated both vertically and horizontally several times to ensure the desired thickness. After hardening the silicone, the mould was removed. After obtaining silicone phantom model, the morphology was measured using micro CT scan and reconfirmed by the validation of morphology.

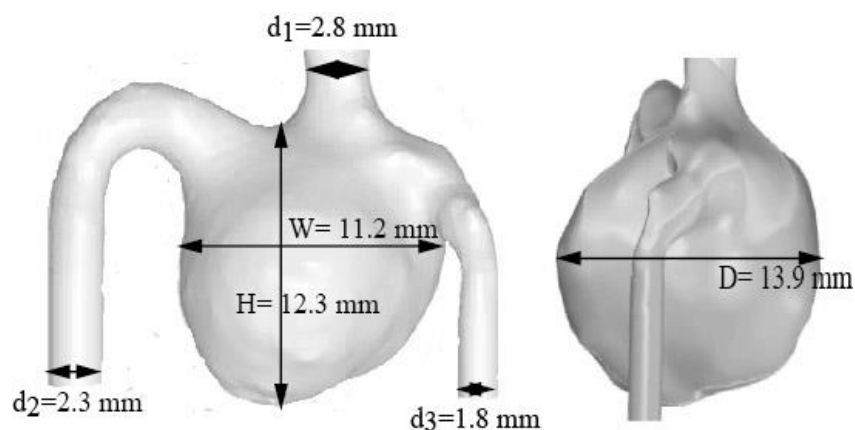


**Fig. 5.** Morphology of middle cerebral aneurysm mould on front and side view core

### 2.2.2 The schematic diagram and full experimental rig

Due to the limitation and constrain in experimental facilities, only velocity and wall shear stress distribution analysis can be made. Thus, validation on velocity distribution at the median plane was done on simulation results, which concluded and validated the overall procedure of the simulation setting and process. Figure 6 illustrates the overall processes of PIV experimental flow circuit.

### 2.2.3 Working fluid properties

To substitute the blood properties, the working fluid namely aqueous Glycerol with sodium (NaI) iodide solution containing 47.38% water, 36.94% glycerol and 15.68% NaI was used [28]. The physical properties were as follows: density of  $\rho = 1188 \text{ kg/m}^3$ , viscosity of  $\nu = 3.57 \times 10^{-6} \text{ m}^2/\text{s}$  and the refractive index of  $n=1.411$ .

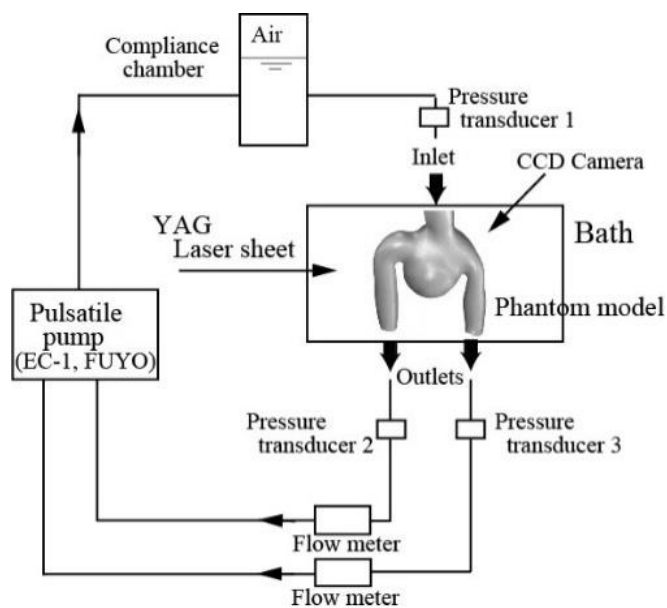


Fig. 6. Schematic PIV setting

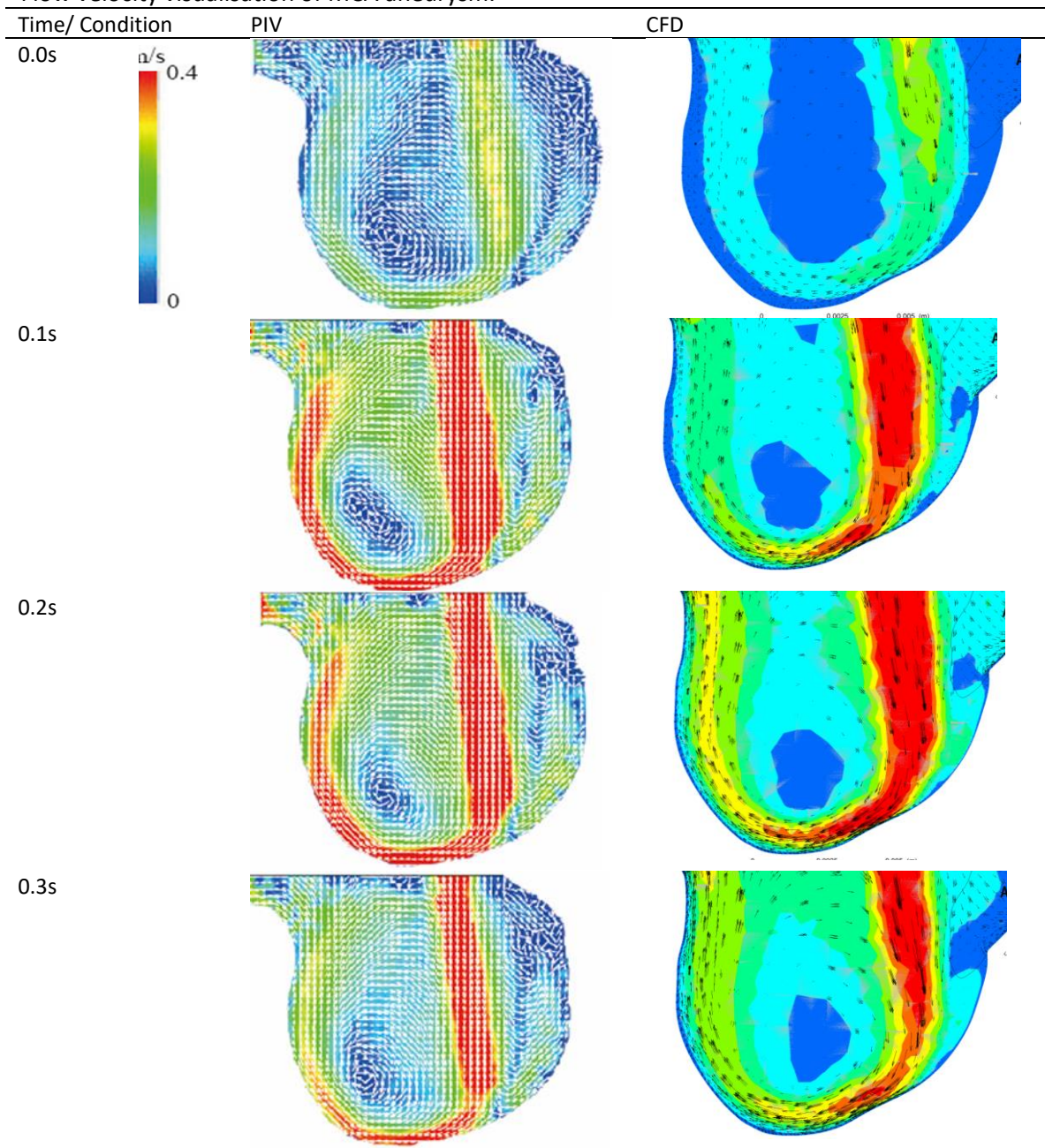
### 3. Results

The velocity, wall pressure, TAWSS, OSI and RRT are discussed on the next subtopic by comparing the flow pattern and behaviour trends at early systole (0.0s) mid - systole (0.1s), peak systole (0.2s) and diastole (0.3s). The relevance and effects of the flow recirculation on this transient flow of patient specific MCA aneurysm to the rupture risk are also addressed.

#### 3.1 Velocity Distribution

Table 2 denotes the velocity distribution during early systole, mid – systole, peak systole and diastole condition in MCA aneurysm obtained from CFD and PIV non-deformation model. The data was taken at four different phases, which were early systole 0.0s, mid – systole 0.1s, peak systole 0.2s, and diastole 0.3s. From the result in Table 2, it can be said that the CFD numerical results was successfully validated with PIV experimental results quantitatively. The velocity data was taken at median plane. The flow entered the bulge with high flow jetting, decreased after hitting the fundus of the aneurysm bulge and started to recirculate. The flow became irregular with few unstable vortices. The formation of recirculation flow at the centre of the flow inside the bulge showed very low velocity with blue coloured area. This was obviously seen during mid-systole to diastole. The blood flow from inlet induced high velocity and flow impingement. This flow recirculation increased due to the increasing of vortex inside the bulge. Then, the flow collided at certain stagnation point and recirculation flow patterns before the velocity became slower once it moved from one phase to another. The location of recirculation happened obviously at the centre of flow and on the side of the stagnation point region, which caused low wall shear stress impact. A low wall shear stress can contribute to high rupture risk of the aneurysm [17]. The flow recirculated in few small parts in anticlockwise and moved away from the stagnation point. Clinically, the disturbance that happens especially on peak and diastole (0.2s and 0.3s) phases can cause high pressure impact, which will weaken the endothelial cells and soften them, which then initiate the rupture to occur. Table 2 explains the evidence of vortex existence in the lower half of the aneurysm area and confirms the development of flow recirculation.

**Table 2**  
 Flow velocity visualisation of MCA aneurysm.



### 3.2 Wall Shear Stress Distribution

Wall shear stress is one of the haemodynamic parameters that relates to the rupturing of MCA aneurysm. WSS is a drag exerted by flowing blood on the arterial wall. Low WSS will cause the vessel to degenerate and weaker, especially when flow recirculation also happens in the bulge area [14]. This may lead to the MCA aneurysm rupture. WSS distribution was varied throughout the cycle. Other than WSS, rupture risk also associated to the oscillatory shear index (OSI) and relative residence time (RRT). The details on WSS distribution with other haemodynamic parameters such as time average WSS (TAWSS) are discussed in this subtopic as far as the WSS was validated with the experimental data. The experiment was done without scaling up the model to ensure better accuracy as shown in Table 3. The trends were seen in good agreement of both WSS values. This result was collected on

the wall of the bleb since this bulge presence changed the haemodynamic indicators on the aneurysm surface. The WSS increased as the velocity flow increases and resulted in the flow impingement [5].

**Table 3**  
 WSS Validation on median plane of MCA aneurysm

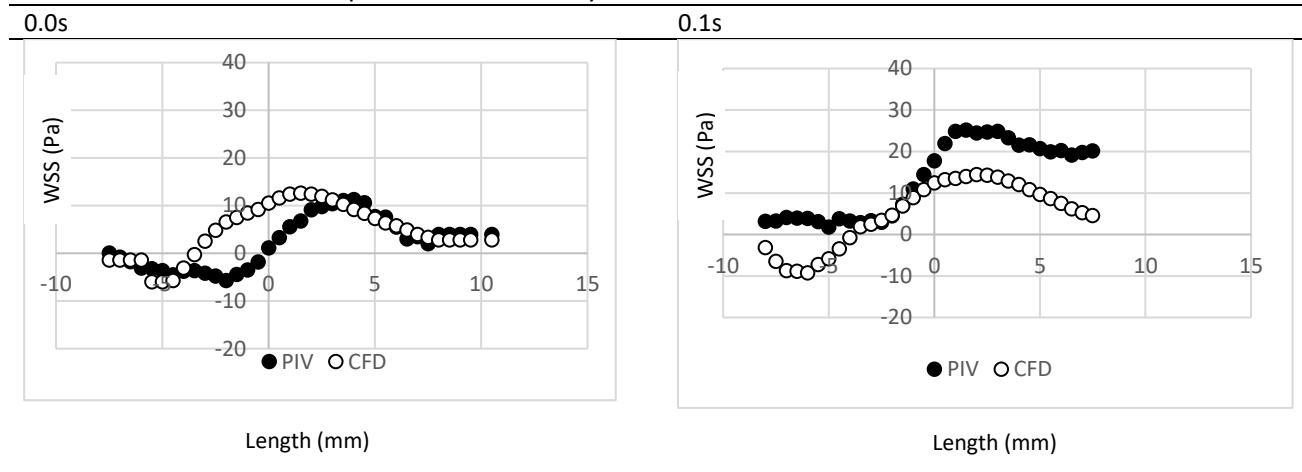
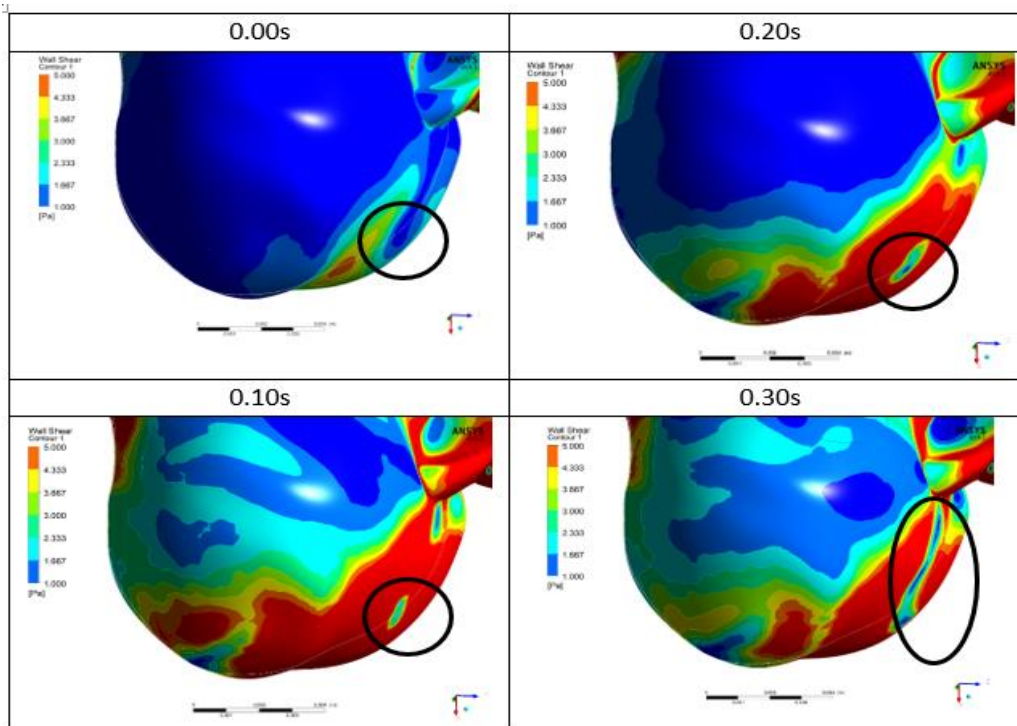


Figure 7 shows the WSS distribution on each phase. The maximum WSS value is important to ensure that lower WSS is able to increase the rupture risk. The threshold of MCA aneurysm rupture was 1 Pa [29]. It was hypothesised that low velocity gives impact to the low WSS and that high OSI influences the increase in aneurysm rupture risk. RRT is advisable to have less than  $10 \text{ Pa}^{-1}$  to avoid atherosclerosis formation, which able to initiate the growth and rupturing of aneurysm. If the percentage of area for RRT with more  $10 \text{ Pa}^{-1}$  is larger, intimal thickening line on the vessel will increase and promote atherosclerosis formation [30]. Figure 8 shows the maximum WSS at each condition and percentage of area with less than 1Pa. As in Figure 8, it was shown that the WSS distribution was set with a range from 1.00 to 5.00 Pa. The blue area indicated the area with low WSS, which was about 4.23% area than 1 Pa during 0.00s, while it decreased to 2.05% on 0.10 s and became 1.01% on 0.2 s and 0.3 s. This MCA aneurysm model is prone to ruptured model; thus, in this situation, high WSS was considered as the high WSS condition can promote early sign to rupturing process as reported by Yoshiki *et al.*, [31]. Even though the low WSS percentage area had decreased, the stagnation region denoted as black circle became bigger, indicating that the existence of flow recirculation at that side had become worse and irregular. This irregularity caused the degeneration of endothelial cells to obviously start at mid - systole 0.1 s. During peak systole, the stagnation point became larger and can slowly burst the weak wall especially during peak systole condition (0.3 s). This was due to the impinging flow and high jetting during peak systole, which then increased the WSS value as shown in Figure 8. The highest WSS was seen during the peak systole 0.2 s, and decreased back during the diastole. During the peak systole, the high WSS distribution region was seen larger (red colour) compared to other phases due to the high jetting inflow velocity in the fluid inside the aneurysm bulge.



**Fig. 7.** WSS distribution on the MCA aneurysm



**Fig. 8.** Maximum WSS distribution

### 3.3 TAWSS, OSI and RRT Effects to Rupture Risk

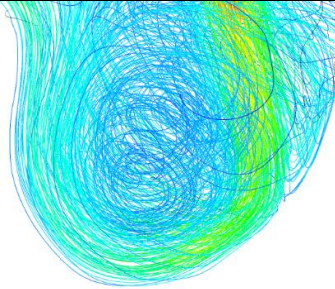
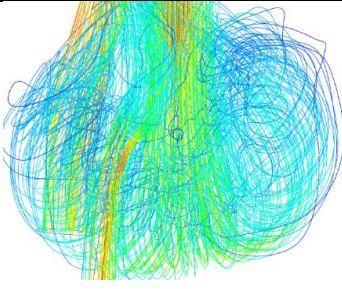
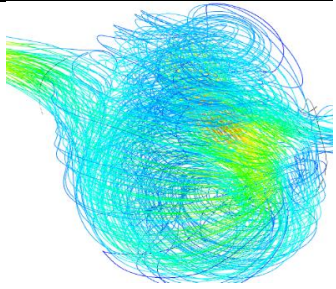
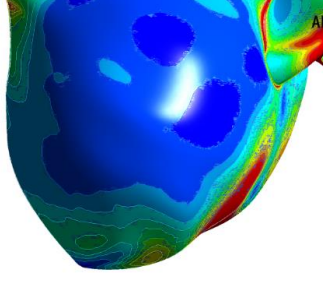
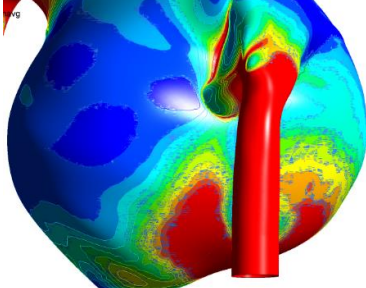
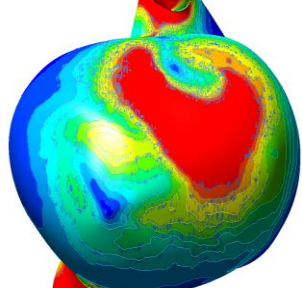
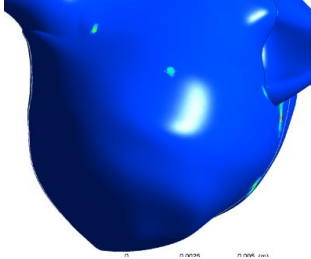
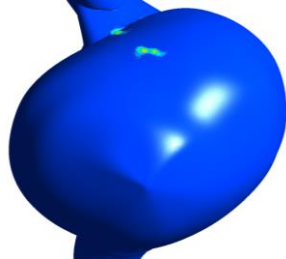
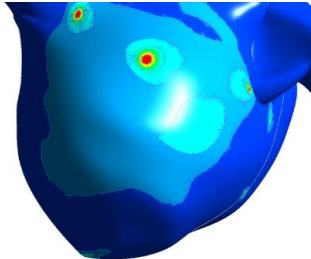
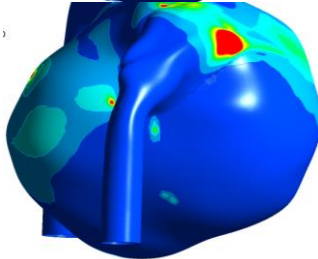
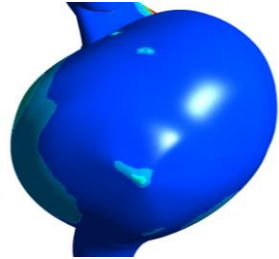
WSS based on Poiseuille's law is a drag exerted by flowing blood on the arterial wall [32,33]. Since this study involved a transient case, WSS was time averaged to get the mean value representing WSS for each cardiac cycle of heartbeat. Thus, TAWSS was calculated to obtain the OSI and RRT values. These parameters are very important as OSI provides an index describing the change in WSS direction other than that of the temporal mean shear stress vector [22,34,35]. The range of OSI for stented artery is from 0 to 0.5. The region with high OSI is predicted to have a high risk of atherosclerosis activity. Since the arterial surfaces with high OSI are prone to atherosclerosis, the desired value of

OSI for lowering rupture risk is from 0.0 to 0.3 [30,36]. Higher OSI is also caused by the high pressure, which can lead to the inflammation on the vessel. This inflammation is not a good sign in an aneurysm and can accelerate the rupture process [36].

RRT is a scalar-valued quantity that indirectly characterises the time amount of atherogenic particles to be in contact with arterial wall. Longer period of contact between atherogenic particles and the arterial wall could cause a high prediction on atherosclerosis formation. The atherogenic activity can be seen through RRT higher than  $10 \text{ Pa}^{-1}$  [30,36]. Therefore, the optimum value of RRT for stented haemodynamic model should be less than or equal to  $10 \text{ Pa}^{-1}$  to avoid any inflammation and high risk of MCA aneurysm rupture [38].

Table 4 discusses the streamline velocity to relate the recirculation flow to the TAWSS, OSI and RRT effects. On the front plane, very low velocity confirmed the recirculation flow that happened on the centre of the aneurysm bulge. This is supported by the TAWSS exerted due to the low velocity, which then exerted the low TAWSS distribution as in second row in Table 4. Reviewing the flow distribution from the side plane and bottom plane supporting the recirculation can be observed to be clearly formed in the aneurysm dome. In Table 4, the percentage lower than 0.5 Pa was about 31.12% area with low WSS. The area was almost 50% with this very low WSS. The size of the stagnation point was similar to that in peak systolic as shown in Figure 7. This site has higher tendency to rupture earlier than at the centre of the dome. From the bottom plane, the flow injected in high velocity and bifurcated the flow into two different sides. This situation also caused higher OSI value at that stagnation area, which can be seen from the side plane on the OSI result. About 1% area of the MCA aneurysm have high OSI value of more than 0.3. It is possible for this small value to spread larger percentage area with high OSI value if no proper treatment is given as soon as possible. The flow that moved to the left side induced larger recirculation region with low velocity and the separation flow to the right part created stagnation point. These two parts showed higher point or interest of the aneurysm to be ruptured due to the flow recirculation effect. On the neck area of the MCA aneurysm, more exceeded RRT threshold value, which was more than  $10 \text{ Pa}^{-1}$  from the side plane, happened at that side with very low velocity and flow recirculation. Almost 0.5% of the total area in the MCA aneurysm dome with more than  $10 \text{ Pa}^{-1}$  have promoted atherosclerosis due to the contact time of atherogenic particles into the surface. This kind of flow behaviour would activate the arteriosclerosis progression and formation. The flow inside the MCA aneurysm was irregular and unstable, which increased the time of contact between the wall and the particles as well as the RRT, leading to higher risk of MCA aneurysm to rupture.

**Table 4**  
 Streamline, TAWSS, OSI and RRT distribution on three different planes

Parameter	Front Plane	Side Plane	Bottom Plane
Streamline Velocity recirculation			
TAWSS Percentage < 0.5 Pa = 31.12%			
OSI Percentage > 0.3 = 1.00 %			
RRT Percentage > 10 Pa <sup>-1</sup> =0.27 %			

### 3.4 Fluid Flow Validation Using PIV Technique

The velocity distribution for CFD and PIV experimental data validated is as shown in Figure 9, which further confirmed that the CFD results can be used to predict velocity distribution in MCA aneurysm and showed similar result with PIV experiment. However, the CFD result obtained was 8% lower than the experimental result. These findings are similar to those described by Ford *et al.*, [39]. In particular, they observed stronger flows and higher velocities in the CFD than those in the PIV models. They also reported that the PIV measurements did not capture detailed flow fields near the wall region and observed disagreements between the CFD and PIV fields in a few regions in the interior of the aneurysm volume away from the walls. Finally, differences in the experimental and computational modelling assumptions could also have introduced discrepancies in the flow fields [39,40]. These results showed a good agreement between CFD and PIV.

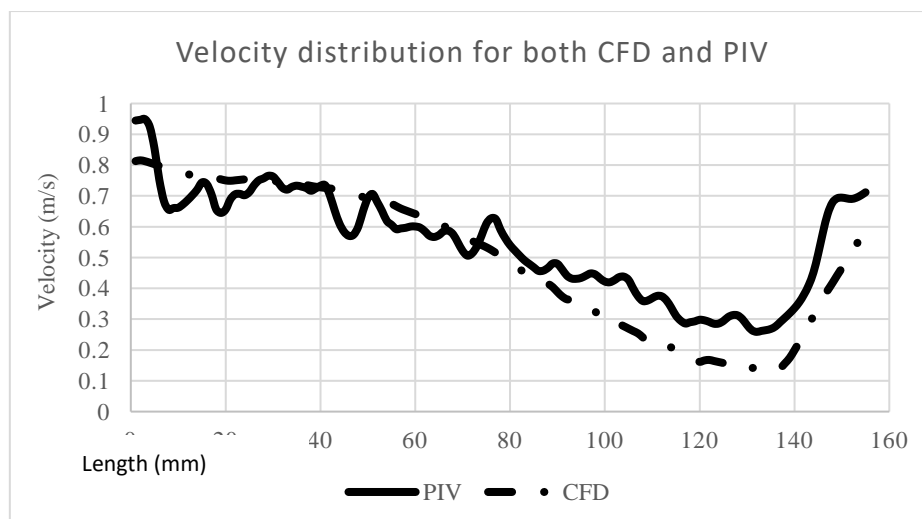


**Fig. 9.** Good agreement of CFD and PIV validation at the centre of the median plane

#### 4. Conclusion

In this study, the transient flow dynamics has been carried out to simulate on a rigid body of a patient-specific MCA aneurysm model and validated using full-scale phantom model by PIV technique. The primary flow from inlet driven a high jetting flow, separated the flow into two parts and formed the flow recirculation, which led to low shear stress, high OSI and longer RRT value. The flow recirculation phenomena were obviously occurred in the centre of the MCA aneurysm dome supported with the larger area with very low WSS value. These situations have actually weakened the endothelial cell lining, injured the surface of the cell with about 1% OSI and 0.27% RRT higher than critical value, which able to promote and initiate atherosclerosis to be formed. The formation of atherosclerosis then led more stagnant particles on the arterial surface and slowly burst the weaken MCA aneurysm wall easily. This is a base study in preparing and completing a guidance system in assessing rupture risk. In conclusion, it is expected that this coming support system can be used as pre-assessment decision making not only for medical consultant, but also for junior medical officers based on the early results as discussed in this paper.

#### Acknowledgement

This research was partially supported by grants with vote number 4F944 Governing Equation for Rupture Prediction in the Middle Cerebral Artery (MCA) Aneurysm, Universiti Teknologi Malaysia (UTM). The authors gratefully acknowledge the contribution and support by the Ministry of Education Malaysia and Research Management Centre, Universiti Teknologi Malaysia. This project was also a collaboration with international joint grant with Institute of Fluid Science (IFS), project code J19I080, Tohoku University Japan. Also, the present work was partially supported by JSPS Science Research Budget #19K04163 and JPJSBP Bilateral Collaborating Research #120199910 in Japan and also grant-in-aid (B) 20H04557. Part of the present work was performed under the Collaborative Research Projects (J17I060 in 2017, J18I108 in 2018, and J19I064 in 2019) of the Institute of Fluid Science, Tohoku University.

## References

- [1] Roth, Carolyn Kaut, and William H. Faulkner Jr. *Review Questions for MRI*. John Wiley & Sons, 2013.
- [2] Inagawa, Tetsuji. "Trends in surgical and management outcomes in patients with aneurysmal subarachnoid hemorrhage in Izumo city, Japan, between 1980-1989 and 1990-1998." *Cerebrovascular Diseases* 19, no. 1 (2005): 39-48.  
<https://doi.org/10.1159/000081910>
- [3] Cebral, Juan R., Marcelo A. Castro, James E. Burgess, Richard S. Pergolizzi, Michael J. Sheridan, and Christopher M. Putman. "Characterization of cerebral aneurysms for assessing risk of rupture by using patient-specific computational hemodynamics models." *American Journal of Neuroradiology* 26, no. 10 (2005): 2550-2559.
- [4] Mut, Fernando, Rainald Löhner, Aichi Chien, Satoshi Tateshima, Fernando Viñuela, Christopher Putman, and Juan R. Cebral. "Computational hemodynamics framework for the analysis of cerebral aneurysms." *International Journal for Numerical Methods in Biomedical Engineering* 27, no. 6 (2011): 822-839.  
<https://doi.org/10.1002/cnm.1424>
- [5] Usmani, Abdullah Y., and K. Muralidhar. "Flow in an intracranial aneurysm model: effect of parent artery orientation." *Journal of Visualization* 21, no. 5 (2018): 795-818.  
<https://doi.org/10.1007/s12650-018-0491-5>
- [6] Andaluz, Norberto, and Mario Zuccarello. "Recent trends in the treatment of cerebral aneurysms: analysis of a nationwide inpatient database." *Journal of Neurosurgery* 108, no. 6 (2008): 1163-1169.  
<https://doi.org/10.3171/JNS/2008/108/6/1163>
- [7] Chalouhi, Nohra, Brian L. Hoh, and David Hasan. "Review of cerebral aneurysm formation, growth, and rupture." *Stroke* 44, no. 12 (2013): 3613-3622.  
<https://doi.org/10.1161/STROKEAHA.113.002390>
- [8] Nathan, Derek P., Chun Xu, Alison M. Pouch, Krishnan B. Chandran, Benoit Desjardins, Joseph H. Gorman III, Ron M. Fairman, Robert C. Gorman, and Benjamin M. Jackson. "Increased wall stress of saccular versus fusiform aneurysms of the descending thoracic aorta." *Annals of Vascular Surgery* 25, no. 8 (2011): 1129-1137.  
<https://doi.org/10.1016/j.avsg.2011.07.008>
- [9] Ngoepe, Malebogo N., Alejandro F. Frangi, James V. Byrne, and Yiannis Ventikos. "Thrombosis in cerebral aneurysms and the computational modeling thereof: a review." *Frontiers in Physiology* 9 (2018): 306.  
<https://doi.org/10.3389/fphys.2018.00306>
- [10] Tominari, Shinjiro, Akio Morita, Toshihiro Ishibashi, Tomosato Yamazaki, Hiroyuki Takao, Yuichi Murayama, Makoto Sonobe et al. "Prediction model for 3-year rupture risk of unruptured cerebral aneurysms in Japanese patients." *Annals of Neurology* 77, no. 6 (2015): 1050-1059.  
<https://doi.org/10.1002/ana.24400>
- [11] Juvela, Seppo. "Prehemorrhage Risk Factors for Fatal Intracranial Aneurysm Rupture." *Stroke: Journal of the American Heart Association* 34, no. 8 (2003): 1852-1857.  
<https://doi.org/10.1161/01.STR.0000080380.56799.DD>
- [12] Zhang, Yu, Hiroyuki Takao, Yuichi Murayama, and Yi Qian. "Propose a wall shear stress divergence to estimate the risks of intracranial aneurysm rupture." *The Scientific World Journal* 2013 (2013).  
<https://doi.org/10.1155/2013/508131>
- [13] Brinjikji, Waleed, Mohammad H. Murad, Giuseppe Lanzino, Harry J. Cloft, and David F. Kallmes. "Endovascular treatment of intracranial aneurysms with flow diverters: a meta-analysis." *Stroke* 44, no. 2 (2013): 442-447.  
<https://doi.org/10.1161/STROKEAHA.112.678151>
- [14] Meng, H., V. M. Tutino, J. Xiang, and A. Siddiqui. "High WSS or low WSS? Complex interactions of hemodynamics with intracranial aneurysm initiation, growth, and rupture: toward a unifying hypothesis." *American Journal of Neuroradiology* 35, no. 7 (2014): 1254-1262.  
<https://doi.org/10.3174/ajnr.A3558>
- [15] Dhar, Sujun, Markus Tremmel, J. Mocco, Minsuok Kim, Junichi Yamamoto, Adnan H. Siddiqui, L. Nelson Hopkins, and Hui Meng. "Morphology parameters for intracranial aneurysm rupture risk assessment." *Neurosurgery* 63, no. 2 (2008): 185-197.  
<https://doi.org/10.1227/01.NEU.0000316847.64140.81>
- [16] Lee, Ui Yun, Jinmu Jung, Hyo Sung Kwak, Dong Hwan Lee, Gyung Ho Chung, Jung Soo Park, and Eun Jeong Koh. "Patient-Specific Computational Fluid Dynamics in Ruptured Posterior Communicating Aneurysms Using Measured Non-Newtonian Viscosity: A Preliminary Study." *Journal of Korean Neurosurgical Society* 62, no. 2 (2019): 183-192.  
<https://doi.org/10.3340/jkns.2017.0314>
- [17] Jing, Linkai, Jixing Fan, Yang Wang, Haiyun Li, Shengzhang Wang, Xinjian Yang, and Ying Zhang. "Morphologic and hemodynamic analysis in the patients with multiple intracranial aneurysms: ruptured versus unruptured." *PLoS One*

- 10, no. 7 (2015): e0132494.  
<https://doi.org/10.1371/journal.pone.0132494>
- [18] Mustaffa, Siti Hajar Adni, Fatimah Al Zahrah Mohd Saat, and Ernie Mattokit. "Turbulent Vortex Shedding across Internal Structure in Thermoacoustic Oscillatory Flow." *Journal of Advanced Research in Fluid Mechanics and Thermal Sciences* 46, no. 1 (2018): 175-184.
- [19] Hamad, A., Syed Mohammed Aminuddin Aftab, and Kamarul Arifin Ahmad. "Reducing flow separation in T-junction pipe using vortex generator: CFD study." *Journal of Advanced Research in Fluid Mechanics and Thermal Sciences* 44, no. 1 (2018): 36-46.
- [20] Cebra, Juan R., Felicitas Detmer, Bong Jae Chung, Joham Choque-Velasquez, Behnam Rezai, Hanna Lehto, Riikka Tulamo et al. "Local hemodynamic conditions associated with focal changes in the intracranial aneurysm wall." *American Journal of Neuroradiology* 40, no. 3 (2019): 510-516.
- [21] Lu, G., L. Huang, X. L. Zhang, S. Z. Wang, Y. Hong, Z. Hu, and D. Y. Geng. "Influence of hemodynamic factors on rupture of intracranial aneurysms: patient-specific 3D mirror aneurysms model computational fluid dynamics simulation." *American Journal of Neuroradiology* 32, no. 7 (2011): 1255-1261.  
<https://doi.org/10.3174/ajnr.A2461>
- [22] Omodaka, Shunsuke, Shin-ichiro Sugiyama, Takashi Inoue, Kenichi Funamoto, Miki Fujimura, Hiroaki Shimizu, Toshiyuki Hayase, Akira Takahashi, and Teiji Tominaga. "Local hemodynamics at the rupture point of cerebral aneurysms determined by computational fluid dynamics analysis." *Cerebrovascular Diseases* 34, no. 2 (2012): 121-129.  
<https://doi.org/10.1159/000339678>
- [23] Taib, Ishkrizat, Shahrin Hisham Amirnordin, Rais Hanizam Madon, Norrizal Mustafa, and Kahar Osman. "The effect of flow recirculation on abdominal aortic aneurysm." In *AIP Conference Proceedings*, vol. 1440, no. 1, pp. 130-135. American Institute of Physics, 2012.  
<https://doi.org/10.1063/1.4704211>
- [24] Shafii, Nadia Shaira, Ryuhei Yamaguchi, Ahmad Zahran Md Khudzari, Gaku Tanaka, Simon Tupin, Atsushi Saitoh Prof Makoto Ohta, and Kahar Osman. "Patient specific images in the middle cerebral artery aneurysm simulation with turbulent model." In *6<sup>th</sup> International Conference on Computational and Mathematical Biomedical Engineering (CMBE2019)*, vol. 2, pp. 635-638, 2019.
- [25] Mahrous, Samar A., Nor Azwadi Che Sidik, and M. Saqr Khalid. "Newtonian and non-Newtonian CFD Models of Intracranial Aneurysm: A Review." *CFD Letters* 12, no. 1 (2020): 62-86.
- [26] Valen-Sendstad, Kristian, Kent-André Mardal, Mikael Mortensen, Bjørn Anders Pettersson Reif, and Hans Petter Langtangen. "Direct numerical simulation of transitional flow in a patient-specific intracranial aneurysm." *Journal of Biomechanics* 44, no. 16 (2011): 2826-2832.  
<https://doi.org/10.1016/j.jbiomech.2011.08.015>
- [27] Yamaguchi, Ryuhei, Taihei Kotani, Gaku Tanaka, Simon Tupin, Kahar Osman, Nadia Shaira Shafii, Ahmad Zahran Md Khudzari et al. "Effects of Elasticity on Wall Shear Stress in Patient-Specific Aneurysm of Cerebral Artery." *Journal of Flow Control, Measurement & Visualization* 7, no. 2 (2019): 73-86.  
<https://doi.org/10.4236/jfcmv.2019.72006>
- [28] Shida, Shuya, Hiroyuki Kosukegawa, and Makoto Ohta. "Development of a methodology for adaptation of refractive index under controlling kinematic viscosity for PIV." In *ASME International Mechanical Engineering Congress and Exposition*, vol. 54884, pp. 313-321. 2011.  
<https://doi.org/10.1115/IMECE2011-64388>
- [29] Goubergrits, Leonid, Jens Schaller, Ulrich Kertzscher, Nils van den Bruck, Kai Pöthkow, Ch Petz, H-Ch Hege, and Andreas Spuler. "Statistical wall shear stress maps of ruptured and unruptured middle cerebral artery aneurysms." *Journal of the Royal Society Interface* 9, no. 69 (2012): 677-688.  
<https://doi.org/10.1098/rsif.2011.0490>
- [30] Chen, Hongmei, Yonghua Bi, Siyeong Ju, Linxia Gu, Xiaoyan Zhu, and Xinwei Han. "Hemodynamics and pathology of an enlarging abdominal aortic aneurysm model in rabbits." *PLoS One* 13, no. 10 (2018): e0205366.  
<https://doi.org/10.1371/journal.pone.0205366>
- [31] Yoshiki, Kenji, Kouichi Misaki, Iku Nambu, Issei Fukui, Masanao Mohri, Naoyuki Uchiyama, and Mitsutoshi Nakada. "Intraoperative rupture of unruptured cerebral aneurysm during craniotomy: a case report." *Case Reports in Neurology* 9, no. 3 (2017): 261-266.  
<https://doi.org/10.1159/000480425>
- [32] Meng, L., H. Yasumoto, and R. Y. L. Tsai. "Multiple Controls Regulate Nucleostemin Partitioning between Nucleolus and Nucleoplasm." *Journal of Cell Science* 119, no. 24 (2006): 5124-5136.  
<https://doi.org/10.1242/jcs.03292>
- [33] Fu, Wenyu, Zhaoyong Gu, Xianlong Meng, Bo Chu, and Aike Qiao. "Numerical simulation of hemodynamics in

- stented internal carotid aneurysm based on patient-specific model." *Journal of Biomechanics* 43, no. 7 (2010): 1337-1342.  
<https://doi.org/10.1016/j.jbiomech.2010.01.009>
- [34] Brindise, Melissa C., Sean Rothenberger, Benjamin Dickerhoff, Susanne Schnell, Michael Markl, David Saloner, Vitaliy L. Rayz, and Pavlos P. Vlachos. "Patient-Specific Cerebral Aneurysm Hemodynamics: Comparison of in vitro Volumetric Particle Velocimetry, Computational Fluid Dynamics (CFD), and in vivo 4D Flow MRI." *arXiv preprint arXiv:1903.01303* (2019): 1-15.
- [35] Aranda, Alfredo, and Alvaro Valencia. "Study on the Relationship Between Wall Shear Stress and Aspect Ratio of Cerebral Aneurysms with Different Pressure Differences Using CFD Simulations." *Journal of Mechanics in Medicine and Biology* 18, no. 05 (2018): 1850055.  
<https://doi.org/10.1142/S0219519418500550>
- [36] Suess, Taylor, Joseph Anderson, Laura Danielson, Katie Pohlson, Tyler Remund, Elizabeth Blears, Stephen Gent, and Patrick Kelly. "Examination of near-wall hemodynamic parameters in the renal bridging stent of various stent graft configurations for repairing visceral branched aortic aneurysms." *Journal of Vascular Surgery* 64, no. 3 (2016): 788-796.  
<https://doi.org/10.1016/j.jvs.2015.04.421>
- [37] Bunney, P. E., A. N. Zink, A. A. Holm, C. J. Billington, and C. M. Kotz. "Orexin activation counteracts decreases in nonexercise activity thermogenesis (NEAT) caused by high-fat diet." *Physiology & Behavior* 176 (2017): 139-148.  
<https://doi.org/10.1016/j.physbeh.2017.03.040>
- [38] Soldozy, Sauson, Pedro Norat, Mazin Elsarrag, Ajay Chatrath, John S. Costello, Jennifer D. Sokolowski, Petr Tvrdik, M. Yashar S. Kalani, and Min S. Park. "The biophysical role of hemodynamics in the pathogenesis of cerebral aneurysm formation and rupture." *Neurosurgical Focus* 47, no. 1 (2019): E11.  
<https://doi.org/10.3171/2019.4.FOCUS19232>
- [39] Ford, Matthew D., Hristo N. Nikolov, Jaques S. Milner, Stephen P. Lownie, Edwin M. DeMont, Wojciech Kalata, Francis Loth, David W. Holdsworth, and David A. Steinman. "PIV-measured versus CFD-predicted flow dynamics in anatomically realistic cerebral aneurysm models." *Journal of Biomechanical Engineering* 130, no. 2 (2008).  
<https://doi.org/10.1115/1.2900724>
- [40] Raschi, Marcelo, Fernando Mut, Greg Byrne, Christopher M. Putman, Satoshi Tateshima, Fernando Viñuela, Tetsuya Tanoue, Kazuo Tanishita, and Juan R. Cebral. "CFD and PIV analysis of hemodynamics in a growing intracranial aneurysm." *International Journal for Numerical Methods in Biomedical Engineering* 28, no. 2 (2012): 214-228.  
<https://doi.org/10.1002/cnm.1459>